Multiple Glass Transitions in Bismuth and Tin beyond Melting Temperatures

Robert F Tournier

X   Type of the Paper (Article.)

Multiple Glass Transitions in Bismuth and Tin beyond Melting Temperatures

Robert F. Tournier

UPR 3228 Centre National de la Recherche Scientifique, Laboratoire National des Champs Magnétiques Intenses, European Magnetic Field Laboratory, Institut National des Sciences Appliquées de Toulouse, Université Grenoble Alpes, F-31400 Toulouse, France.

*   Correspondence: robert.tournier@lncmi.cnrs.fr

Abstract: Liquid-liquid transitions were discovered above the melting temperature (T_m) in Bi and Sn up to $2T_m$ and viewed as glass transitions at $T_g = T_{n+} > T_m$ of composites nucleated at $T_x < T_m$ and fully melted at T_{n+}. A glassy fraction (f) disappeared at 784 K in Sn. (T_{n+}) increases with singular values of (f) depending on T_x with (f) attaining 100% at $T_g = T_{n+} = 2T_m$. The nonclassical model of homogeneous nucleation is used to predict T_x, T_{n+} and the specific heat. The singular values of (f) leading to (T_{n+}) correspond to percolation thresholds of configurons in glassy phases. A phase diagram of glassy fractions, occurring in molten elements is proposed. The same value of (T_x) can lead to multiple (T_g). Values of ($T_g = T_{n+}$) can be higher than ($2T_m$) for $T_x/T_m < 0.7069$. A specific heat equal to zero is expected after cooling from $T \leq 2T_m$ and could correspond to a fully ordered phase. Weak glassy fractions are nucleated near (T_{n+}) after full melting at (T_m) without transition at (T_x). Resistivity decreases were observed after thermal cycling between solid and liquid states with weak and successive values of (f) due to $T_x/T_m < 0.7069$.

Keywords: Metals, glass transitions, melting enthalpy, Liquid-liquid transitions, density, first-order transitions, configurons, Phase 3, structural transitions.

Publisher's Note: MDPI stays neutral with regard to jurisdictional claims in published maps and institutional affiliations.

1. Introduction

Liquid–liquid phase transitions occur in glass-forming melts at temperatures T_{n+} above T_m, the equilibrium thermodynamic melting transition of crystals [(1) (2) (3) (4) (5) (6) (7) (8) (9) (10; 11) (12) (13) (14) (15) (16) (17) (18) (19; 20) (21) (22)]. These transitions often result from the separation of two liquid states, occurring in all supercooled materials at a temperature $T_x < T_m$, including pure elements in which two liquid phases of the same composition coexist. A liquid fraction crystallizes at T_x and melts at T_m while the complementary glassy fraction melts at $T_{n+} = T_g$ [(23) (24) (22)]. The purpose of this publication is to relate all the liquid-liquid transitions, occurring above the melting temperature (T_m) in Bi and Sn up to ($2T_m$), and beyond, to glass transition temperatures [(1) (3) (4)]. A weak glassy fraction disappeared at 784 K in Sn as recently observed with specific heat measurements [5]. Here, we recall that (T_{n+}) increases with singular values of (f) depending on T_x and we examine if (f) can attain 100% at $T_g = T_{n+} = 2T_m$ in Bi and Sn as already envisaged for a component of $Cu_{46}Zr_{46}Al_8$ melt [(23) (12)].

Molecular dynamics simulations were employed to study the thermodynamics and kinetics of the glass transition and crystallization in deeply undercooled liquid Ag and Ag-Cu at high cooling rates of the order of 10^{12} K/s [(25) (26)]. A first order transition from the

liquid-phase (L) to a metastable, heterogeneous, ordered phase viewed as a glass phase 40
called G-phase was observed. The L-G transition occurred by nucleation of the G-phase 41
from the L-phase. The lowest glass transition temperature of liquid-phase (L) depends on 42
its Lindemann coefficient and is much weaker than the nucleation temperature of G-phase 43
[(27) (28) (29) (30)]. Increasing the heating rate increased the glass transition temperature 44
of liquid (L). A first order transition from liquid (L) to G-glass was observed, when a su- 45
percooled liquid evolved isothermally below its melting temperature at deep undercool- 46
ing [(26)]. Several simulations of G-phases in various elements showed full melting heat 47
H_m at various temperatures T_{n+} = T_g in Ag [(25)], in Zr [(31)], in Cu and in Fe [(32)]. The 48
values of T_{n+} were determined from singular values of G-phase frozen enthalpy, employ- 49
ing the nonclassical homogeneous nucleation (NCHN) model to predict T_x, T_{n+} and the 50
enthalpy. Singular values of (f) leading to (T_{n+}) correspond to percolation thresholds of 51
broken bonds (configurons) leading to glassy phases up to T_{n+} [(33) (34) (24) (29) (30)]. 52

High undercooling rates of bulk liquid elements are known since many years [(35)]. 53
Consequently, we plan to confirm, in this publication, that the nucleation of G-phases and 54
their glass transition temperatures above T_m are observable without employing heating 55
and cooling rates of the order of 10^{10} to 10^{13} K/s to escape from crystallization. A phase 56
diagram of glassy fractions, occurring in molten elements at $T_x < T_m$, is proposed, complet- 57
ing the diagram already established for $T_x > T_m$ [(30)] in agreement with previous molec- 58
ular dynamics simulations [(25) (26) (31) (32)]. The specific heat values at T_g = T_{n+} is pre- 59
dicted up to T_g = 2 T_m where a fully ordered glassy phase is expected. The density far above 60
T_m depends on the formation time of bonds increasing glassy phase fractions. Resistivity 61
decreases are due to the increase in (f) in these liquids [(4)]. 62

2. Diagram of glassy phases 63

Three liquid states are present in all melts with enthalpies equal to $\varepsilon_{ls}H_m$, $\varepsilon_{gs}H_m$ and 64
$\Delta\varepsilon_{lg}H_m$ [(36)]. For liquid elements, that are easily crystallized, the liquid enthalpy coeffi- 65
cients obey to the following [(30), (27)]: 66

$$\varepsilon_{ls} = \varepsilon_{ls0}\left(1 - \frac{\theta^2}{\theta_{0m}^2}\right) = \varepsilon_{ls0}(1 - 2.25\,\theta^2), \qquad (1) \quad 67$$

68

$$\varepsilon_{gs} = \varepsilon_{gs0}\left(1 - \theta^2/\theta_{0g}^2\right) = \varepsilon_{gs0}(1 - \theta^2) \qquad (2) \quad 69$$

70

$$\Delta\varepsilon_{lg}(\theta) = \left[\varepsilon_{ls} - \varepsilon_{gs}\right] = [\varepsilon_{ls0} - \varepsilon_{gs0} - \theta^2(2.25\,\varepsilon_{ls0} - \varepsilon_{gs0})], \qquad (3) \quad 71$$

72

where H_m is the melting enthalpy, ε_{ls} and ε_{gs} are fractions of H_m, θ_{0m} = -2/3 and θ_{0g} = -1 are 73
the reduced Vogel-Fulcher-Tammann (VFT) temperatures in liquid elements for which 74
the minimum value of T_g is fixed by the Lindemann coefficient (δ_{ls}) of each element [(27)]. 75
Eq. (3) is transformed into Eq. (4) for the minimum value of ε_{ls0} = ε_{gs0}: 76

77

$$\Delta\varepsilon_{lg} = -1.25\,\varepsilon_{gs0}\,\theta_g^2, \qquad (4) \quad 78$$

where $\Delta\varepsilon_{lg}(\theta_g)$ is the latent heat coefficient, accompanying the glass transition during 79
the first cooling, the formation of Phase 3 below the percolation threshold of bonds, and 80
the partial breaking of bonds after reheating above T_g, occurring without latent heat [(30)] 81
Figure 3. These relaxation effects due to the development of bonds below the percolation 82

threshold at T_g are observed after quenching melt in amorphous state and heating at 20 K/min [(37), (38) (39) (40) (41) (42)].

Coefficient minima ($\varepsilon_{lso} = \varepsilon_{gso}$) were initially determined to be equal to 0.217 [(43)]. They were the average of many liquid element coefficients deduced from the undercooling rate of each of them corresponding to the mean value 0.103 of their Lindemann coefficient [9,18]. The number 2.25, initially equal to 2.5 in Eq. (1), had for consequence to fix the VFT temperature to $T_m/3$ [(44)]. It appears later that ($\Delta\varepsilon_{lg}$) in Eq. (3) is the enthalpy coefficient of a true thermodynamic phase called 'Phase 3' discovered for the first time in supercooled water [(45) (46) (47)]. It is now a generic name, attributed to all glassy phases, which are formed through a first-order transition [(37)]. Phase 3 could be the congruent bond lattice predicted for disordered oxide systems [(48)], extended later to critical packing density formation applied to broken bonds (configurons) producing the glass transitions at T_g [(33), (49)]. An ordered fraction of atoms equal to various percolation thresholds exists up to T_{n+}, in all glass-forming melts [(34; 50; 23)]. Phase 3 results from the formation of configuron phases [(50)]. The NCHN model predicted the formation conditions of glacial phases (Phase 3) in Ag-Cu and Ag liquids at various heating rates as previously described by molecular dynamics (MD) simulations, showing full melting at $T_{n+} = 1.119T_m$ for Zr, $1.126T_m$ for Ag, $1.219T_m$ for Fe and $1.354T_m$ for Cu [(25) (26) (31) (32)]. These phenomena are governed by singular values of the enthalpy $\Delta\varepsilon_{lg}$ of glassy Phase 3, formed at nucleation temperatures T_{nG} [(29), (30)].

Two families of nucleation temperatures are given in Eqs. (5,6) where θ_{n-} is equal to two opposite values of θ_g because ε_{gs} is a function of θ^2 in Eq. (2):

$$\theta_{n-} = \theta_g = \frac{\pm(\varepsilon_{gs}-2)}{3}, \tag{5}$$

$$\theta_{n+} = \Delta\varepsilon \tag{6}$$

where $\Delta\varepsilon$ is equal to singular values of the enthalpy coefficient (-$\Delta\varepsilon_{lg}$) of Phase 3.

There are two methods to produce a glassy phase with an enthalpy coefficient equal to (-$\Delta\varepsilon$). The first one predicts the undercooling temperature for each value of $\Delta\varepsilon$. These nucleation temperatures (θ_x) are calculated using the (NCHN) model applied to Liquid 2:

$$\varepsilon_{gs}(\theta = 0) = (3\theta_x + 2 - \Delta\varepsilon)/(1 - \frac{\theta_x^2}{\theta_{0g}^2}) \tag{7}$$

Here, $\theta_{0g}^2 = 1$. For $\Delta\varepsilon = 0$, a second order-like phase transition temperature takes place at T_g during heating for the minimum value of ε_{gs0}. Values of θ_x for various values of $\Delta\varepsilon$ are deduced for the same value of ε_{gs0}.

Glass phases, formed at θ_x after undercooling, lead to glassy phases with $\theta_g = \theta_{n+} = \Delta\varepsilon$ in agreement with Eq. (6). They are accompanied by a crystallized fraction (1-$\Delta\varepsilon$). A composite crystal-glass is built below T_m with a melting enthalpy (1-$\Delta\varepsilon$) H_m and a missing enthalpy ($\Delta\varepsilon$ H_m) recovered at T_{n+} [(23)]. The glassy phase fraction is not destroyed at T_m and depends on the sample thermal history and the last value of $\Delta\varepsilon$ obtained at T_x during heating.

The minimum glass transition at T_g is masked by spontaneous crystallization of many liquid elements and determined with Eq. (7) using $\Delta\varepsilon = 0$ and the minimum value of $\varepsilon_{gso} = \varepsilon_{lso}$, depending on the Lindemann coefficient δ_{ls} of each element [(27)]:

$$\varepsilon_{gs0} = \varepsilon_{ls0} = (1 + \delta_{ls})^2 - 1 \tag{8}$$

In Figure 1, a second method is used to calculate new values of θ_x during heating. Each value of θ_g varying from -0.5 to 2 corresponds to a value of T_g/T_m between 0.5 and 3. All ratios T_g/T_m, represented in Figure 1, could be those of phases resulting from a first-order transition at T_x, with T_x and T_g depending on heating rates. Applying Eq. (7), determines the value of $\varepsilon_{gs0} = \varepsilon_{ls0}$, (positive or negative [(23)]), for each (θ_g) and $\Delta\varepsilon = 0$. Each first-order transition at θ_x respects $\Delta\varepsilon = \theta_{n+} = \theta_g > 0$, in agreement with Eq. (6). Negative values

of θ_g ($T_g/T_m < 1$) are higher than θ_x because T_g/T_m is always higher than T_x/T_m. The values 132
of (θ_x) obtained with Eq. (7) are weaker than those predicted in Figure 1 along the dashed 133
curve. 134

135

Bi and Sn glassy phase diagram

136
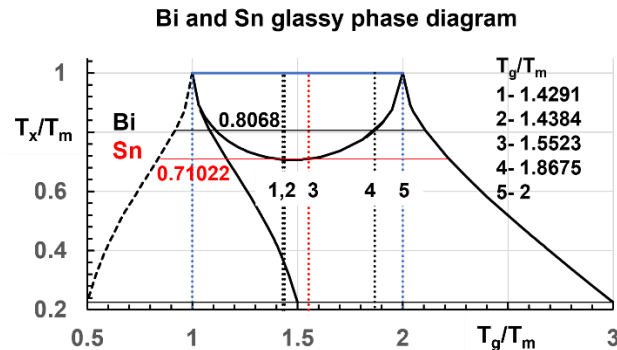
Figure 1: Glassy phase diagram (T_g/T_m) resulting from first-order transitions at T_x/T_m during heating of liquid elements. 137
Valuable for all glass transitions due to Lindemann coefficients. For Bi, $T_x/T_m = 0.8068$ reveals $T_g/T_m = 1.8675$ as observed 138
from differential thermal analysis (DTA). For Sn, $T_x/T_m = 0.71022$ reveals $T_g/T_m = 1.5523$. For $T_x/T_m > 0.7069$, there are 5 139
glass transitions. For $T_x/T_m < 0.7069$, the number of glass transitions is equal to 3. (T_g/T_m) can be higher than 2. Transitions 140
at $T_g/T_m = 1.4291$ and 1.4384 are initiated by other (T_x/T_m) values. $T_g/T_m = 0.5$, 1.5 and 3 for $T_x/T_m = 0.22451$. For $T_x/T_m = 1$, 141
transitions were observed at T_g/T_m with latent heat much weaker than ($\Delta\varepsilon H_m$) above T_m. 142

143

The two lines between $T_g/T_m = 0.5$ and 1.5 are symmetrical with respect to 1. There 144
are 5 values of T_g/T_m for T_x/T_m higher than 0.7069, and 3 values of T_g/T_m for $T_x/T_m < 0.7069$, 145
depending on the singular values of $\Delta\varepsilon$ determined by each thermal history. For $T_x/T_m = $ 146
0.7069, $T_g/T_m = 1.475$. Note that the NCHN model predicts nucleation temperatures at T_{n+} 147
$> 2\ T_m$, ignoring the structure of these new ordered phases. We assume that glassy phases 148
are formed. 149

150

3. Diagram applications 151

Liquid-liquid transitions in bismuth were observed along lines (1, 2, 4, 5) in Figure 1, 152
by several authors using differential scanning calorimetry (DSC) or differential thermal 153
analysis (DTA) at various heating rates, leading, in fact, to vitreous transitions at $T_g/T_m = $ 154
1.4291, 1.4384, 1.8675 and 2 for $T_x/T_m = 0.70811$, 0.70767, 0.80681 and 1 respectively without 155
recovery of the endothermic heat ($\Delta\varepsilon H_m$) at these temperatures [(1) (3) (4)]. The value of 156
ε_{gs0} for bismuth was equal to 0.1907 corresponding to $\delta_{ls} = 0.0912$ [4]. 157

The vertical lines (3,5) in Figure 1 are those of tin and correspond to $T_g/T_m = 1.5523$ 158
($T_g = 783.9$ K) and 2 ($T_g = 2\ T_m$). The horizontal line $T_x/T_m = 0.71022$ determines $T_g/T_m = $ 159
1.5523. Two liquid-liquid transitions, occurring at $T_g/T_m = 1.5523$ and 2 are known up to 160
now. Only $T_g/T_m = 1.5523$ is characterized as a glass transition [(5)]. 161

The Bi glass transition was not reproduced at $T_g/T_m = 2$ during cooling because all 162
bonds were erased during heating far above $T_g/T_m = 2$ as observed with heating and cool- 163
ing rates of 2 K/min [(4)] (Figure 13b). 164

In contrast, the Sn transition at $T_g/T_m = 2.168$, during heating, disappeared during 165
cooling and gave rise to a new transition at $T_g/T_m = 1.832$ characterizing a first-order tran- 166
sition at $T_g/T_m = 2$ observing that [(2.168+1.832)/2 = 2] with heating and cooling rates of 7.5 167
K/min [(4)] (Figure 13e). The first-order transition at $T_g/T_m = 1.832$ ($T_g = 652$ °C) was re- 168
produced during the second heating and cooling at 10 °C/min and could correspond to $\Delta\varepsilon$ 169
= 0.832. 170

The resistivity [(4)] after the second heating were much weaker than those obtained 171
during the first heating of Sn and Bi. At the highest temperature $T = 2.28\ T_m$, the ordered 172

fractions did not disappear because T_g is expected to be on the order of 3 T_m. The resistivity decreases were equal to 22% for tin and 16.7% for Bi.

4. Singular enthalpy coefficients

We examine the case where the glassy phase is formed at T_x. Characteristic values of $\Delta\varepsilon_{lg}$ (θ) = -$\Delta\varepsilon$ at various temperatures T_x would correspond to various percolation thresholds of configurons. The enthalpy coefficient ($\Delta\varepsilon_{lg}$ = -$\Delta\varepsilon$) of Phase 3 is constant up to T_{n+} = T_g. The transition at T_g leads to a new liquid state with $\Delta\varepsilon_{lg}$ linearly decreasing with temperature in agreement with Eq. (6). Consequently, the melt specific heat, being proportional to the derivative ($\Delta\varepsilon_{lg}$/dT), undergoes a jump equal to $\Delta\varepsilon H_m/T_m$ at T_g = T_{n+}.

4.1 Bismuth

The weakest glass transition temperature of bismuth was predicted at T_g = 202.46 K [(23)]. The singular enthalpy coefficients $\Delta\varepsilon$ were determined: $\Delta\varepsilon_{lg}$ = 0, $\Delta\varepsilon_{lg0}$ = 0.1907, -$\Delta\varepsilon_{lg}$ (θ_g) = 0.094065, -$\Delta\varepsilon_{lg}$ (θ_{0m} = -2/3) = 0.10594, -$\Delta\varepsilon_{lg}$ (θ = -1) = 0.238375 and $\Delta\varepsilon$ = -1. The experimental coefficients ($\Delta\varepsilon$) giving rise to θ_{n+} = 778/544.5 -1 = 0.429 and 784.6/544.5-1 = 0.44096 were obtained with a heating rate of 5 K/min and were nearly equal to the theoretical values (0.42908 = 0.1907+0.23838) and (0.43838 = 0.094065+0.10594+0.23838) [(1)]. In Figure 2, these two transitions are nucleated at T_x = 286.2 and 288 K during undercooling. Only the transition at T = 286.2 K is represented, leading to the horizontal line (2) up to T_g = 778.1 K. The observed coefficient $\Delta\varepsilon$ = 0.8675 [(3)], nucleated at T = 370 K, was equal to the sum (0.42908+0.43838) up to T_g = 1016 K along Line (3) [(23)]. The coefficient ($\Delta\varepsilon$ = 1) along Line (4), nucleated at 395 K, without crystallization at T_m, disappears at T_g = 2T_m = 1089 K. We expect, by reversing heating to cooling at a reduced temperature slightly lower than T_g, that the enthalpy coefficient $\Delta\varepsilon_{lg}$ will fall to zero, without forgetting that the glassy fraction is equal to $\Delta\varepsilon$.

The enthalpy coefficient variation of Phase 3 along Line (5) in Figure 2, obeying to Eq. (6), is obtained after a transition at T_g = T_{n+} followed by continuous heating through the various glass transitions.
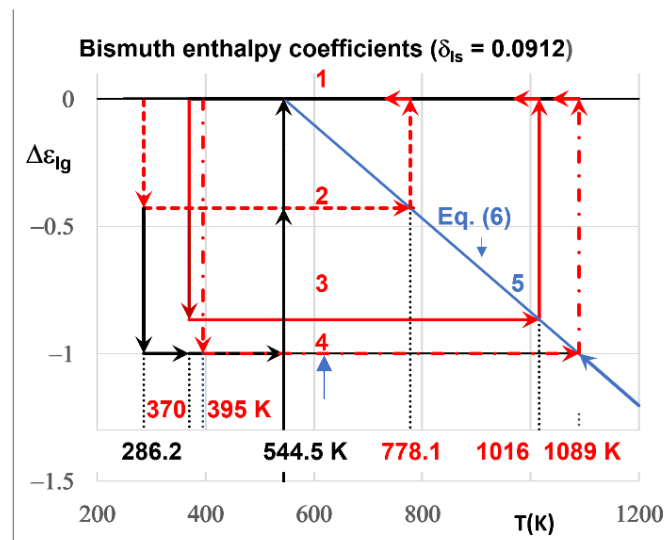

Figure 2: Bismuth glassy phase fractions f = $\Delta\varepsilon$ expected after undercooling and reheating. Four liquid-liquid transitions at T_{n+} = T_g after reheating were observed. Horizontal lines: 1- $\Delta\varepsilon_{lg}$ = 0 of glassy fractions; 2- $\Delta\varepsilon$ = θ_{n+} = θ_g = 0.42908 up to T_g = 778 K, 0.43838 up to T_g = 783 K, (not represented); 3- $\Delta\varepsilon$ = 0.8675 up to T_g = 1016 K; 4- $\Delta\varepsilon$ = 1 up to T_g = 1089 K without crystallization at T_m. Vertical lines: T_x = 286.2 K leading to $\Delta\varepsilon$ = 0.42908 and a crystallized fraction (1-$\Delta\varepsilon$ = 0.57092); T_x =

370 K leading to $\Delta\varepsilon = 0.8675$ and a crystallized fraction $(1-\Delta\varepsilon = 0.1325)$; $T_x = 395$ K leading to $\Delta\varepsilon = 1$; $T_m = 544.5$ K: melting of crystallized fractions; $T_{n+} = 778.1$ K; $T_{n+} = 1016$ K; $T_{n+} = T_g = 2T_m = 1089$ K. The glass transitions leading to $\Delta\varepsilon_{lg} = 0$ could be observed by reversing heating to cooling slightly below T_g. Line (5) represents Eq. (6).

4.2 Tin

The weakest glass transition temperature of tin is $T_g = 185.2$ K ($\theta_g = -0.63332$), applying Eq. (7) for $\Delta\varepsilon_{gs0} = 0.167$, ($\delta_{ls} = 0.08028$). The singular enthalpy coefficients of liquid tin are $\Delta\varepsilon_{lg} = 0$, $\Delta\varepsilon_{lg0} = 0.167$, $-\Delta\varepsilon_{lg}(\theta_g) = 0.08373$, $-\Delta\varepsilon_{lg}(\theta_{0m} = -2/3) = 0.09278$, $-\Delta\varepsilon_{lg}(\theta = -1) = 0.20875$ and $-\Delta\varepsilon_{lg} = 1$. A sum of all basic coefficients leads to $\Delta\varepsilon = 0.5523$. Here too, the combination of singular enthalpy coefficients determines the glass transition at T_g/T_m.
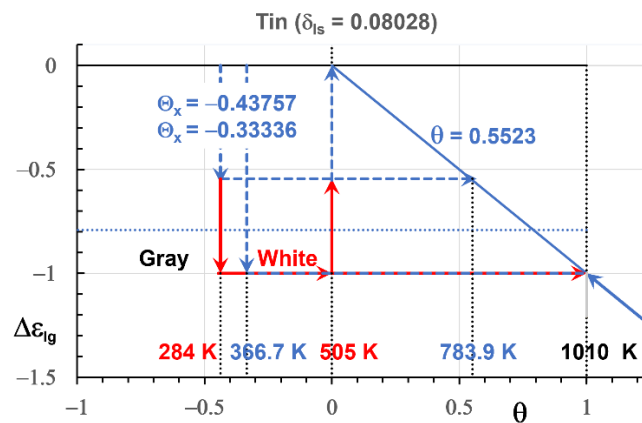
Figure 3: Tin glassy phase fraction $f = \Delta\varepsilon$ expected after undercooling and reheating. $T_x = 284$ K ($\theta_x = -0.43757$), leading to a liquid-liquid transition at $T_{n+} = T_g = 783.9$ K after reheating. ($\Delta\varepsilon = 0.5523$) corresponding to the enthalpy coefficient of the gray phase. The crystallized fraction $(1-\Delta\varepsilon)$ of the white phase is (0.4477). The glassy phase with $T_g = 2 T_m = 1010$ K and $\Delta\varepsilon = 1$ is nucleated at $T_x = 366.7$ K ($\theta_x = -0.33336$) and heated without crystallization at T_m.

In Figure 3, the transition occurring at $T_x = 284$ K ($\theta_x = -0.43757$) gives rise to a glassy fraction $f = 0.5523$ and a glass transition at $T_g/T_m = 1.5523$ ($T_g = 783.9$K) calculated with $\varepsilon_{gs0} = 0.167$ and Eqs. (6,7). The temperature (284 K) separates two crystalline phases corresponding to gray and white tin. The temperature $T_x = 284$ K, corresponding to the melting temperature $T_m \cong 284$ K of gray tin, is difficult to observe because of the concomitant formation of a glass phase at the same temperature [(51)]. Above 284 K, the liquid fraction of gray phase is a glass with $T_g = 783.9$ K, coexisting with a crystallized fraction $(1-0.5523 = 0.4477)$ of white tin up to T_m. A glass transition temperature was observed in tin at $T_g \cong 780$ K, confirming the existence of a glassy fraction above T_m [(5)]. The glass phase corresponding to $f = \Delta\varepsilon = 1$ would be nucleated at $T_x = 366.7$ K and heated without crystallization at T_m, up to $T_g = 2 T_m = 1010$ K. We will see that the glass transition at 1010 K observed by resistivity measurements is reversible [(4)].

As a conclusion of this chapter, the existence of singular glassy fractions (f) in liquid Bi and Sn is predicted. Liquid-liquid transitions are observed and occur at the predicted glass transition temperatures.

5. Experimental densities of Bi and Sn during heating

Density varies linearly with increasing temperature, T (K), above T_m in liquid elements [(3) (51) (52) (53) (54) (55)]:

$$d = d_0 - aT. \tag{9}$$

where d_0 is a density at 0 K. In general, density measurements were made after melting the crystalline phase in the absence of temperature T_x resulting from undercooling and

reheating. Nevertheless, liquid-liquid transitions were observed with heating rates be-
tween 0.1 and 20°C/min at temperatures (T_{n+}) [(23)]. Consequently, new atomic bonds are
induced by relaxation of liquid state near T_{n+} [(22)]. The singular coefficient $\Delta\varepsilon$ belonging
to lower enthalpy phases determines the temperature $T_{n+} = T_g$, and gives rise, at very low
heating rate, to relaxation of weak endothermic latent heat in the neighborhood of tem-
peratures T_{n+}. These relaxation times also have for consequence, to disperse the liquid
density measurements and are due to the development of bonds above T_m. Density, d, is
expected to be reduced for bismuth and increased for tin by this enthalpy relaxation up to
$T_g = 2T_m$. Then, Eq. (9) can be written as a function of $\theta = \Delta\varepsilon$, applying Eqs. (4,6):

$$d = d_0 - aT_m\left(1 + \theta_{n+}\right) = d_0 - aT_m\left(1 \pm \Delta\varepsilon_{lg}\right). \qquad (10)$$

Density measurements would lead to dispersed results because they would be dependent
on the measurement time and on the amplitude of the relaxed enthalpy.

5.1 Bismuth density

The specific heat of bismuth above T_m, measured point after point [(56)], is strongly
dispersed as reproduced in Figure 4. Few singular values of T_{n+} are indicated. The deepest
one occurs at 862 K ($\Delta\varepsilon = 2\times0.23838 +0.10594 =0.5827$) and the highest ones at 1017 K ($\Delta\varepsilon =$
0.8675) and 1089 K ($\Delta\varepsilon = 1$). The specific heat (0.147 J/K/g) at T_m is recovered at 1180 K
showing that the transition width at 1089 K is about 100 K in this case. These results show
that the dispersion of measurements attains 12 % and that these weak glassy fractions
induced by relaxation, have glass transition temperatures equal to T_{n+}. Consequently, liq-
uid-liquid transitions observed around each temperature T_{n+} would correspond to frac-
tions much weaker than the singular value ($\Delta\varepsilon$) associated with T_{n+}. The same dispersion
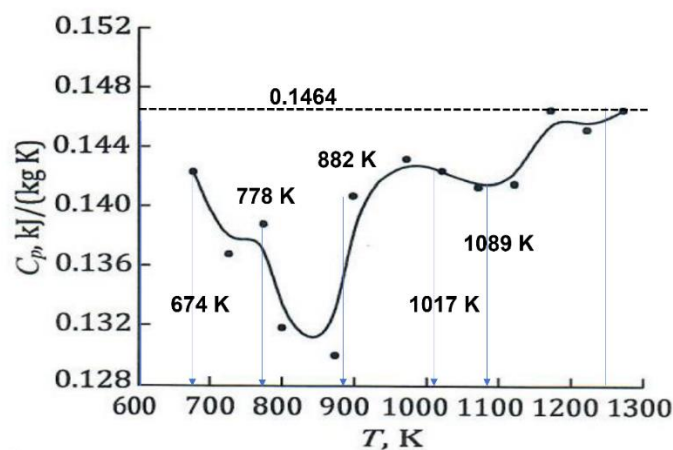is expected for density measurements below the line defined by Eq. (9}.

Figure 4: Specific heat of bismuth above T_m. Reproduced from [(56)] with permission of Springer Ed. The line $C_p =$
0.1464 KJ/ (Kg K) leading to the value of C_p at $T_m = 505$ K is added. The specific heat is constant from T_m to $2 T_m$ in the
absence of relaxed enthalpy. $T_g = 674$ K for $\Delta\varepsilon = 0.23838+0.09401 = 0.3324$, $T_g = 778$ K for $\Delta\varepsilon = (0.42908 = 0.1907+0.23838)$,
$T_g = 882$ K for $\Delta\varepsilon = (0.429+0.23838+0.09456 = 0.761)$, $T_g = 1017$ K for $\Delta\varepsilon = 0.8675$, $T_g = 1089$ K for $\Delta\varepsilon = 1$.

The density of liquid bismuth was measured by gamma attenuation from the melting
point to 1000 °C in discrete steps of 5 °C and reproduced in Figure 5 [(3)]. Values of den-
sity were stabilized at singular coefficients, 0.42908, 0.8093 and 0.90594, each of them being
a sum of basic coefficients corresponding to a glassy phase. A transition between 0.8093
and 0.90594, occurring at 1.8675 T_m (743.8 °C) was observed by DTA at 0.1 °C/min.
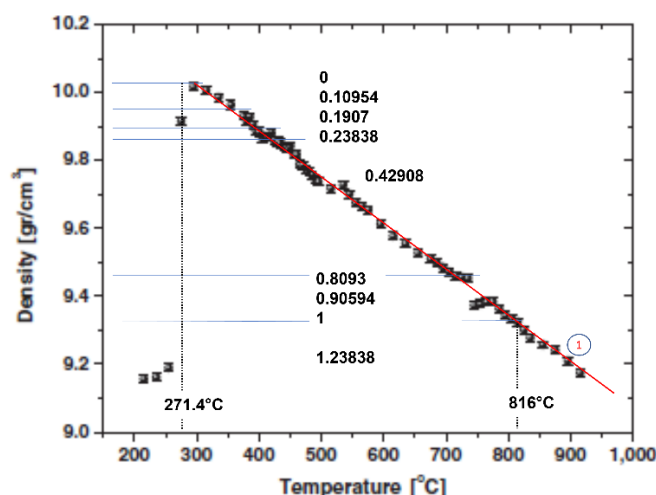
Figure 5: Bismuth density versus temperature, T (°C). Reproduced with authorization of EPL, EPI [(3)]. The density variation between T_m (K) and 2 T_m (K) is equal to the density change at T_m while the enthalpy coefficient varies from 0 to 1. Singular values of the enthalpy coefficient are added to the original figure. Line (1) is the density before enthalpy relaxation of glassy phases. A melting heat, 1.23853 H_m includes the latent heat of the glassy fraction occurring for T_g/T_m = 1 in the phase diagram of Figure 1.

The density change at T_m corresponds to a melting heat of 1.23838 H_m instead of H_m, because it contains the enthalpy (0.23838 H_m) given by Eq. (4), which corresponds to the initial formation of Phase 3. There is no visible transition in Figure 5 at T = 2T_m as shown by the quasi-continuity of the density.

5.2 Tin density

The density of tin is represented Lines (1-3) in Figure 6: solid tin, Line (1) [(54)], and liquid tin, Lines (2) [(53)] and (3) [(57)]. Lines (2,3) are chosen among measurements with only 50 Kg/m³ of error reviewed by Alchagirov and Chochaeva [(53)]. The difference in density, 82 Kg/m³ at 2 T_m is higher than the measurement error. Lines (2,3) could represent two liquid densities that are parallel and separated by approximately 75 Kg/m³ or less inside the measurement error. This phenomenon, if confirmed, would be associated with the presence of a weak glassy fraction f << 0.20875 from 0 K to 2 T_m and beyond as predicted. The density change at T_m and the melting heat depend on the thermal history and may include glassy fractions that are melted at very high temperatures beyond 3 T_m as predicted by the glassy phase diagram.
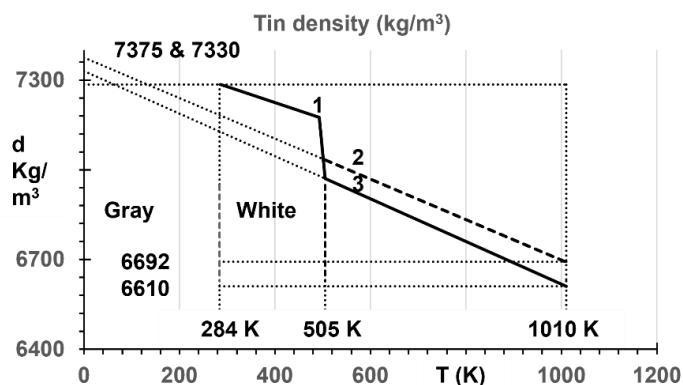
Figure 6: Tin density (d) in Kg/m³, versus T (K). Line (1) [(54)]; Line (2) [(53)]; Line (3) [(57)]. T_x = 284 K, the glass formation temperature after undercooling and the melting temperature of gray tin. 2 T_m = 1010 K.

6. The heat capacities during heating

The specific heat (C_P) is reduced by a contribution (δC_P) above T_m during heating in the presence of a glassy fraction f = $\Delta\varepsilon$ after an enthalpy change (-$\Delta\varepsilon$ H_m) and a first-order transition at T_x:

$$\delta C_p = T\,(\delta S/\delta\theta)_p\,(\delta\theta/\delta T)_p = -TS_m/T_m \tag{11}$$

where $S = -\Delta\varepsilon\,H_m/T_m = -\theta\,H_m/T_m$ represents the entropy of the glassy phase fraction at T_{n+} with $\Delta\varepsilon = \theta$, applying Eq. (6). There is no specific heat and density added in the absence of glassy fraction for $\Delta\varepsilon = 0$ in all liquids. Eq. (11) is not applied in the absence of first-order transition at T_x.

Applying Eq. (11) leads to $C_p = 0$ at $T_g = 2\,T_m$:

For Sn:

$$C_p = 28.43 - 0.0563 \times (T - T_m), \tag{12}$$

with H_m = 7179 J/mole [(58)] and T_m = 505 K

At T_m, C_p = 28.43 J/mole in agreement with Chen's measurements [(59)] after adding 0.9 mJ/mole corresponding to the electronic specific heat contribution of tin [(60)].

For Bi:

$$C_p = 30.2 - 0.05546(T - T_m), \tag{13}$$

with T_m = 544.5 K. At T_m, C_p = 30.2 J/mole [(61)] is used to determine H_m = 8613 J/mole. The measured melting enthalpy is 1.23838 H_m leading to 10662 J/mole inside an uncertainty of measurements varying from 10480 to 11300 J/mole [(62)].

The constants 28.43 and 30.2 J/K/mole are values of C_p at T_m in the absence of glassy phases. These heat capacities are equal to zero at T = 2T_m and to 28.43 and 30.2 J/mole at temperatures higher than 2T_m as shown for Sn in Figure 7 and bismuth in Figure 8. When a fraction (f) of liquid is no longer in a glassy state above the temperature (T), (C_p) linearly decreases from 28.43 for Sn to zero and from 30.2 J/K/mole to zero for Bi. These specific heat variations, expected during heating, are plotted as a function of temperature for Sn and Bi in Figures 7 and 8.
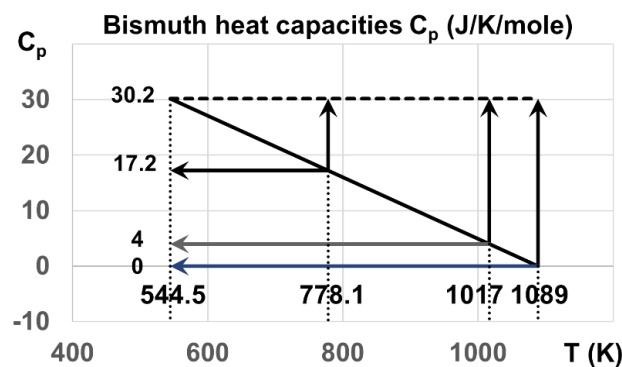
Figure 7: Heat capacities of bismuth in J/K/mole. C_P = 30.2 from T = 544.5 to 1089 K in the absence of glass phase. C_P = 17.2 from T_m = 544.5 to T_g = 778.1 K in the presence of glassy fraction f = 42.908 %. C_P = 4 from T_m = 544.5 to T_g = 1017 K in the presence of a glassy fraction f = 86.75 %. C_P = 0 for f = 100%. Heating beyond T_g, leads to C_P = 30.2 inside the transition width. Cooling from a temperature slightly below T_g leads to the glassy state.
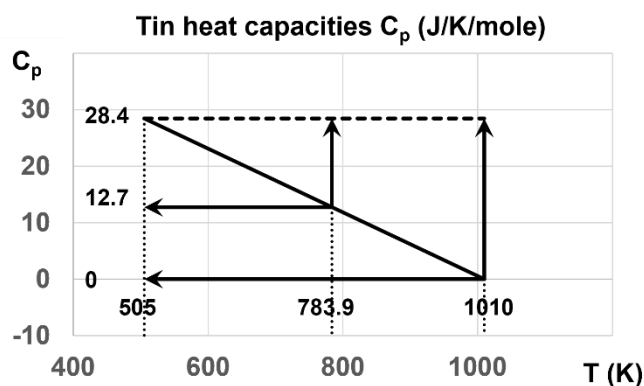
Figure 8: Heat capacities of tin in J/K/mole. C_P = 28.43 from T = 505 to 1010 K in the absence of glassy phase. C_P = 12.7 from T_m = 505 to T_g = 783.9 K in the presence of glassy fraction f = 55.23%. C_P = 0 for f = 100%. Heating beyond T_g, leads to C_P = 28.43 inside the transition width. Cooling from a temperature slightly below T_g leads to the glassy state.

7. Other experimental observations of glassy states above T_m

7.1 Tin

A glass transition was detected for the first time around 783.9 K in agreement with our predictions [(5)]. This transition induced a specific heat jump of about 1.8 J/K/mole instead of 12.7 J/K/mole corresponding to a glassy fraction f $\cong$ 1.8/28.4 = 6.3 % instead of 55.23 %. This glassy fraction was induced in a stepwise-scanning mode: the temperature during the thermal equilibration stage changed with time and gradually approached a constant value in about 60 minutes. The peak of $\Delta C_{P,}$ observed during this slow heating, accompanied by critical phenomena, could be attributed to the thermodynamic transition of configurons [(33), (63)]. The jump of ΔC_P measured at 4 K/min was weaker because the nucleation time of new bonds was much lower.

7.2 Bismuth

DTA at 0.1 °C/min reveals an endothermic latent heat of the order of 20 to 100 J/mole [(3)] at T_g =1.8675 T_m. A transition width (ΔT) of 200 K was observed at 1089 K by resistivity measurements with 2°C/min and a width (ΔT = 10 K) expected for R = 0.1°C/min [(4)]. We attribute this liquid-liquid transition to a glassy fraction of the order of 6.6 % with 20 J/mole and 33 % with 100 J/mole] assuming a transition width of 10 K. A second endothermic heat was observed by DTA at T = 2 T_m = 1089 K corresponding to a second glass transition and to the enthalpy relaxed during 720 min between 1017 and 1089 K.

Configuron thermodynamic transition was revealed by structural changes at the glass transition via radial distribution functions [(64), (65)]. The first sharp diffraction minimum in the pair distribution function was shown to contain information on structural changes in amorphous materials at the glass transition temperature (T_g). An additional feature of such configuron transition was determined by measuring the temperature

dependence of the structure factor of molten bismuth, -S(q). The authors observed, in their
neutron diffraction analysis [(3)] , an additional feature in the measurement that appeared
around the melting temperature of bismuth. Pair distribution function curves (g(r)) were
calculated for each (S(q)) measurement. At and above melting, both the S(q) and g(r) curves
were characterized by a shoulder located on the high q and r side of the first peak,
respectively. The temperature dependence of the coordination numbers lead to the
number of atoms contributed by the shoulder, $N_{Shoulder}(T)$. The derivative of $N_{Shoulder}$ with
respect to temperature, showed a discontinuity at the transition point at 1089 K, and was
associated with this temperature-driven transformation and a structural change. This
structural change is a signature of the thermodynamic transition of configurons [(33)].

7.3 BiSb20 wt%

DSC revealed that C_P was equal to zero at 1070 °C with a heating rate of 20 °C /min
[(4)] Figure 15b. From our model, we deduce that the glassy fraction (f) was 100 %. The
liquidus temperature of this alloy is 425 °C (698 K). The glass transition, occurring at
1070 °C (1343 K), was weaker than $2 T_m = 1396$ K. The specific heat increased from 1070 °C
to 1123 °C. The transition width (2000 K) is expected to be 10 times wider than at 2 K/min.
Consequently, the recovery of ΔC_P, for a temperature increase of 53 K, is of the order of
$53/2000 \cong 2.6$ % of its value at T_m. We conclude that the glassy fraction (f = 100 %) was
induced at a temperature $T_x < T_m$. The rapid increase of the heating rate had for conse-
quence to induce the first order transition at $T_x < T_m$. This experiment showed for the first
time that a glassy phase of 100 % can be obtained with a heating rate of 20 K/min.

7.4 InSn80wt%

An internal friction method was used to study the structural changes of InSn80wt%
[(66)]. This alloy has a melting temperature of about 190°C (463 K) and a glass transition
temperature, expected at $2 T_m = 926$ K (653 °C). A minimum of internal friction occurs at
625 °C et un maximum at 700 °C. Based on the results of a diffraction experiment around
700 °C, the liquid structures before and after the peak are very different [(4)]. Before the
change, there are residual covalent bonds of solid tin in the melt and during the transition,
the residual bonds are broken and at the same time, new atomic bonds build up, with a
relatively uniform melt forming. This description given by [(4)] is known as being due to
the percolation threshold of configurons [(33)].

7.5 PbSn61.9wt%

This eutectic composition has a melting temperature of 183 °C (456 K). The highest
glass transition temperature is predicted at 912 K (639 °C). The internal friction has a max-
imum at 670 °C and a minimum at 560 °C with a heating rate of 2.5 °C/min and a maxi-
mum at 712 °C and a minimum at 600 °C with 6 °C/min. This liquid -liquid transition
temperature increases with the heating rate as observed in all glasses [(4)].

7. Another method to stabilize glassy states above (2 T_m)

A process was described by Zu F.Q. [(4)], ignoring at this time, that resistivity de-
creases could be due to the formation of glassy fractions, added after several cooling to
various temperatures $T_x < T_m$, followed by successive reheating as shown in Figure 7. Each
value of $T_x/T_m < 0.7069$ lead to a glass transition much higher than $2 T_m$ as shown by the
glassy phase diagram of Figure 1. These various reheating enriched the total glassy fraction
as shown by resistivity reductions of 40 % after three heating of Cu-Sb76.5wt%, of 22 % in
tin and 16.7% in bismuth after two heating. In addition, depending on heating rate, another
glass transition occurs at $T_m < T_{n+} < 2 T_m$ in various alloys such as InSn80wt%, InBi32wt%

at R = 3°C/min, and CuSb76.5wt% at 5°C/min. They were due to the formation of very weak glassy fractions (f), depending on heating and cooling rates. The residual resistivity is equal to 100 $\mu\Omega$.cm at T_m during the first heating. Consequently, the formation of high glassy fractions with $T_g \gg 2 T_m$ could be attained after adding new thermal cycles, leading to a maximum resistivity fall. Reheating cycles could stabilize the glassy phase above (T_{n+} = $2T_m$).
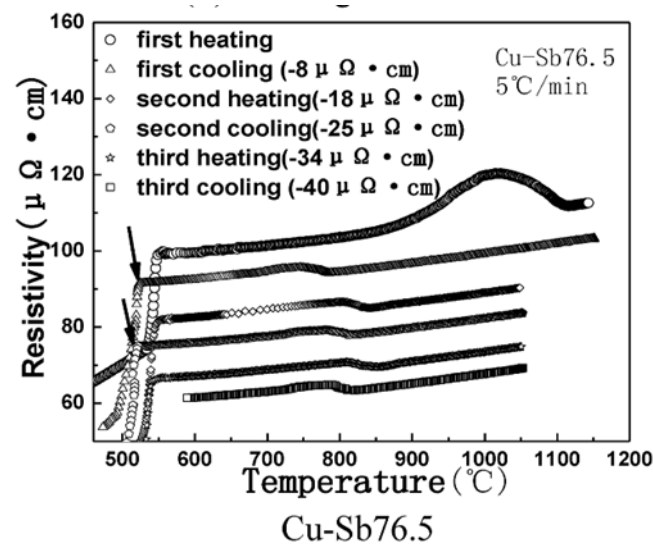
Figure 9: Resistivity falls of Cu-Sb 76.5 wt% after thermal cycling. Reproduced from [(4)] (Figure 13f).

8. Conclusions

Liquid-liquid transitions are observed below and above T_m.

First-order transitions, predicted by the NCHN model, occur at $T_x < T_m$, building glassy phase fractions ($\Delta\varepsilon$) after supercooling and crystallized fractions (1-$\Delta\varepsilon$) of melt. Melting of glassy fractions occurs at temperatures $T_{n+} > T_m$ at the percolation threshold of configurons (broken bonds). One of them induces a glass enthalpy equal to the melting enthalpy ($\Delta\varepsilon$ = 1), without crystallized fraction, up to a glass transition ($T_g = 2T_m$). All glassy fractions would have a heat capacity equal to zero, revealed by reversing heating to cooling below T_{n+}.

Liquid-liquid transitions between the melting temperature (T_m) and ($2 T_m$) are observed in the absence of first order transition at $T_x < T_m$ and are reminiscent of glassy fractions (f) formed at temperatures (T_x) weaker than (T_m) through first-order transitions. These weak fractions correspond to singular values ($\Delta\varepsilon$) of enthalpy coefficients ($\Delta\varepsilon_{lg}$ (θ) = -$\Delta\varepsilon$) of a new phase called "Phase 3", and to typical percolation thresholds of configurons at various temperatures ($T_{n+} = T_g$). These fractions are slowly induced near (T_{n+}) by relaxation in the absence of first order transition prior to melting.

Several situations are encountered in bismuth and tin:

1. After melting Bi and Sn at T = T_m, weak fractions (f) were built by slow heating (0.1°C/min for Bi and one hour between each measurement for Sn) and melted at $\theta_g = \theta_{n+} = (T_{n+} - T_m)/T_m$ = $\Delta\varepsilon$. Liquid-liquid transitions were observed at 1.8675 T_m for bismuth and 1.5523 T_m for Sn. The glassy character of these transitions is confirmed by structural transitions that we attribute to melting of configurons. The glass transition in Sn was also characterized by a weak specific heat jump predicted by the NCHN model and a peak at 1.5523 T_m due to the thermodynamic character of a transition obeying to critical exponents associated with

configuron percolation. There is no endothermic latent heat equal to ($\Delta\varepsilon$ H_m), only a weak endothermic heat equal to a weak fraction (f << $\Delta\varepsilon$).

2- After melting Bi and Sn at T = T_m, transitions were also observed at T = 2 T_m by DTA and (or) resistivity that we consider as new glass transitions. The transition was reversible only for Sn. A weak endothermic heat was observed for Bi at 2 T_m, as expected for a weak value of (f).

3- We show that the density variation between T_m and 2 T_m is equal to that from solid to liquid at T_m. The glassy state of Bi has a density equal to that of the liquid at T_m while, that of Sn is equal to that of the solid at T_m.

4- After melting Bi at T = T_m, high-resolution measurements of the density showed the existence of singular values corresponding to those of the enthalpy of Phase 3. The melting heat at T_m corresponds to 1.23838 H_m instead of H_m including, in addition, the latent heat of glassy phase after the first cooling as predicted by the NCHN model.

5- A glassy phase diagram is proposed for systems having their lowest transition determined by their Lindemann coefficients. Each first order transition at $T_x < T_m$ leads to multiple glass transitions. The possible existence of weak glassy fractions (f) for $T_x/T_m < 0.7069$, with glass transition temperatures much higher than (2 T_m) is envisaged (beyond (3 T_m) for f < 22.45%). Resistivity measurements showed decreases in Bi and Sn from T_m to 2 T_m and beyond, after thermal cycling between the solid and undercooled liquid states.

6- The glassy phase formations at T_x are accompanied by latent heats, being recovered at T_{n+} with ($T_m < T_{n+} < 2T_m$) which decrease the liquid specific heat. Predictions of their contribution equal to (θ_{n+} H_m/T_m) are proposed for $T_{n+} = T_g \leq 2T_m$. The heat capacity linearly decreases down to zero when $\Delta\varepsilon$ increases up to 1 ($T_{n+} = 2T_m$). A specific heat equal to zero, down to T_m, could be induced by reversing heating to cooling from a temperature slightly weaker than $T_g = T_{n+}$. We show, for the first time, that the liquid specific heat is constant between T_m and $2T_m$ in the absence of glassy phase.

7- The stability of glassy fractions for $T_x/T_m < 0.7069$ can be very high because their (T_g) could be much higher than (2 T_m) as proved by resistivity decreases observed up to 2 T_m and beyond in Bi and Sn. The glassy fraction (f) is enhanced by successive thermal cycles between solid and liquid states. Each new glassy fraction could be added and could reinforce the total glassy fraction at very high temperatures up to f ≤ 100%.

References

1. **Wang L., Bian X., Liu J.** Discontinuous structural phase transition of liquid metal and alloys. *Phys. Lett. A.* 2004, Vol. 326, pp. 429-435.

2. **Yue Y.** Experimental evidence for the existence of an ordered structure in a silicate liquid above its liquidus temperature. *J. Non-Cryst. Sol.* 2004, Vol. 345 & 346, pp. 523-527.

3. **Greenberg, Y., et al.** Evidence for a temperature-driven structural transition in liquid bismuth. *EPL.* 2009, Vol. 86, p. 36004.

4. **Zu, Fang-Qiu.** Temperature-Induced Liquid-Liquid Transition in Metallic Melts: A Brief Review on the New Physical Phenomenon. *Metals.* 2015, Vol. 5, pp. 395-417.

5. **Xu, L. et al.** Folded network and structural transition in molten tin. *Nature Comm.* 2022, Vol. 13, p. 126.

6. **Wang J., Li J., Hu R., Kou H., Beaugnon E.,.** Evidence for the structure transition in a liquid Co-Sn alloy by in-situ magnetization measurement. *Mater. Lett.* 2015, Vol. 145, pp. 261-263.

7. **He Y-X., Li J., Wang J., Kou H., Beaugnon E.** Liquid-liquid structure transition and nucleation in undercooled Co-B eutectic alloys. *Applied Physics A.* 2017, Vol. 123, p. 391.

8. **He Y.-X., Li J.-S, Wang J., Beaugnon E.** Liquid-liquid structure transition in metallic melt and its impact on solidification: a review. [ed.] Elsevier. *Trans. Nonferr. Met. Soc. China.* 2020, Vol. 30 (9), pp. 2293-2310.

9. **Qiu X., Li J., Wang J. , Guo T., Kou H., Beaugnon E.,.** Effect of liqui-liquid structure transition on the nucleation in undercooled Co-Sn eutectic alloy. *Mater.Chem. and Phys.* 2016, Vol. 170, pp. 261-265.

10. **Bennett, T.D., et al.** Melt-quenched glasses of metal-organic frameworks. *J. Am. Chem. Soc.* 2016, Vol. 138, pp. 3484-3492.

11. **Wang J., He Y., Li J., Li C., Kou H., Zhang P., Beaugnon E.** Nucleation of supercooled Co melts under a high magnetic field. *Mater. Chem. Phys.* 2019, Vol. 225, pp. 133-136.

12. **Zhou C., Hu L., Sun Q., Qin J., Brian X., and Yue Y.** Indication of liquid-liquid phase transition in CuZr-based melts. *Appl. phys. Lett.* 2013, Vol. 103, p. 171904.

13. **Kim Y.H., Kiraga K., Inoue A., Masumoto T., and Jo H.H.** Crystallization and high mechanical strengthof Al-based amorphous alloys. *Materials Trans.* 1994, Vol. 35, pp. 293-302.

14. **Hu Q., Sheng H.C., Fu M.W., Zeng X.R.** Influence of melt temperature on the Invar effect in (Fe71.2B.024Y4.8)96Nb4 bulk metallic glasses. *J. Mater. Sci.* 2019, Vol. 48, pp. 6900-6906.

15. **P.S. Popel, O.A. Chikova, and V.M. Matveev.** Metastable colloidal states of liquid metallic solutions. *High Temp. Mater. & Proc.* 1995, Vol. 4, pp. 219-233.

16. **Jiang H-R, Bochtler B., Riegler X.-S. , Wei S.S., Neuber N., Frey, M., Gallino I., Busch R., Shen J.** Thermodynamic and kinetic studies of the Cu-Zr-Al(-Sn) bulk metallic glasses. *J. All. Comp.* 2020, Vol. 844, p. 156126.

17. **Wei S., Yang F., Bednarcik J., Kaban I., Shuleshova O., Meyer A. & Busch R.** Liquid-liquid transition in a strong bulk metallic glass-forming liquid. *Nature Commun.* 2013, Vol. 4, p. 2083.

18. **Lan S., Ren Y., Wei X.Y., Wang B., Gilbert E.P., Shibayama T., Watanabe S., Ohnuma M., & Wang X.-L.** Hidden amorphous phase and reentrant supercooled liquid in Pd-Ni-P metallic glass. *Nat. Commun.* 2017, Vol. 8, p. 14679.

19. **Yang, B., et al.** Dependence of crystal nucleation on prior liquid overheating by differential fast scanning calorimeter. *J. Chem. Phys.* 2014, Vol. 140, p. 104513.

20. **Xu W. , Sandor M.T., Yu Y., Ke H.-B., Zhang H.P., Li M.-Z, Wang W.-H., Liu L. & Wu Y.** Evidence of liquid-liquid transition in glass-forming La50Al35Ni15 melt above liquidus temperature. *Nat. Commun.* 2015, Vol. 6, p. 7696.

21. **Chen E.-Y., Peng S.-X.. Peng, Michiel M.D., Vaughan G.B.M., Yu Y., Yu H.-B., Ruta B., Wei S., Liu L.** Glass-forming ability correlated with the liquid-liquid transition in Pd42.5Ni42.5P15 alloy. *Scripta Materialia.* 2021, Vol. 193, pp. 117-121.

22. **Tournier R.F. and Ojovan M.I.** Building and breaking bonds by homogenous nucleation in glass-forming melts leading to three liquid states. *Materials.* 2021, Vol. 14, p. 2287.

23. **Tournier, R.F. and Ojovan, M.I.** Multiple melting temperatures in glass-forming melts,. *Sustainability.* 2022, Vols. 14,, p. 2351.

24. **Tournier R.F.** Liquid-liquid transitions due to melting temperatures of residual glassy phases expected in Pt57Cu23P20. *Aspects Min. Miner. Sc.* 2022, Vol. 8(5), pp. 979-989.

25. **An Q. Johnson W.L., Samwer K., Corona S.L., and Goddard III W. A.** First-order transition in liquid Ag to the heterogeneous G-Phase. *J. Phys. Chem. Lett.* 2020, Vol. 11, pp. 632-645.

26. **An Q. Johnson W.L., Samwer K., Corona S.L., Goddart III W.A.** Formation of two glass phases in binary Cu-Ag liquid. *Acta Mater.* 2020, Vol. 195, pp. 274-281.

27. **Tournier R.F.** Lindemann's rule applied to the melting of crystals and ultra-stable glasses. *Chem. Phys. Lett.* 2016, Vol. 651, pp. 198-202. Corrig: Chem. Phys. Lett. 675 (2017) 174.

28. **Vopson M.M., Rugers N., Hepburn I.** The generalized Lindemann Melting coefficient. *Sol. State Commun.* 2020, Vol. 318, p. 113977.

29. **Tournier R.F.** Validation of non-classical homogeneous nucleation model for G-glass and L-glass formations in liquid elements with recent molecular dynamics simulations. *Scripta Mater.* 2021, Vol. 199, p. 113859.

30. **Tournier, R.F. and Ojovan, M.I.** Prediction of second melting temperatures already observed in pure elements by molecular dynamics simulations. *Materials.* 2021, Vol. 14, p. 6509.

31. **Becker S., Devijver E., Molinier R., and Jakse. N.** Glass-forming ability of elemental zirconium. *Phys. Rev. B.* 2020, Vol. 102, p. 104205.

32. **Bazlov A.I., Louzguine-Luzguin D.V.** Crystallization of FCC and BCC liquid metals studied by molecular dynamics simulation. *Metals.* 2020, Vol. 10, p. 1532.

33. **Ojovan M.I.** Ordering and structural changes at the glass-liquid transition. *J. Non-Cryst. Sol.* 2013, Vol. 382, p. 79.

34. **Hasmy A., Ispas S., Hehlen B.** Percolation transitions in compressed SiO_2 Glasses. *Nature.* 2021, Vol. 599, p. 65.

35. **P. Vinet, L. Magnusson, H. Frederikssen, P.J. Desré.** Correlations between surface and interface energies with respect to crystal nucleation. *J. Colloid Interf. Sci.* 2002, Vol. 255 (2), pp. 363-374.

36. **Tournier R.F.** Fragile-to-fragile liquid transition at Tg and stable-glass phase nucleation rate maximum at the Kauzmann temperature,. *Physica B,.* 2014, Vol. 454, pp. 253-271.

37. —. First-order transitions in glasses and melts induced by solid superclusters nucleated by homogeneous nucleation instead of surface melting. *Chem. Phys.* 2019, Vol. 524, pp. 40-54.

38. **Jian Q.K., Wang X.D., Nie X.P., Zhang G.Q., Ma H. , Fecht H.J., Bendnarck J. , Franz H., Liu Y.G., Cao Q.P., Jiang J.Z.** Zr-(Cu,Ag)-Al bulk metallic glasses. *Acta Mater.* 2008, Vol. 56, pp. 1785-1796.

39. **Hu, C., Zhang, C. and Yue, Y.** Thermodynamic anomaly of the sub-Tg relaxation in hyperquenched metallic glasses. *J. Chem. Phys.* 2013, Vol. 138, p. 174508.

40. **Wang, L.-M., Borick, S. and Angell, C.A.** An electrospray technique for hyperquenched glass calorimetry studies: propylene glycol and di-n-butylphthalate. *J. Non-Cryst. Sol.* 2007, Vol. 353, pp. 3829-3837.

41. **Inoue, A. and Zhang, T.: Masumoto, T.** The structural relaxation and glass transition of La-Al-Ni and Zr-Al-Cu amorphous alloys with a significant supercooled liquid region. *J. Non-Cryst. Sol.* 1992, Vol. 150, p. 396.

42. **L. Hornboll, L. and Y., Y. Yue.** Enthalpy relaxation in hyperquenched glasses of different fragility. *J. Non-Cryst. Sol.* 2008, Vol. 354, pp. 1832-1870.

43. **Tournier R. F.** Presence of intrinsic growth nuclei in overheated and undercooled liquid elements. *Physica B.* 2007, Vol. 392, pp. 79-91.

44. **Perepezko, J.H. and Paik, J.S.** *Rapidly solidified amorphous and crystalline alloys.* [ed.] B.H. Kear, B.G. Gessen and M. Cohen. New York : Elsevier Science, 1982. pp. 42-63.

45. **R.F. Tournier.** Predicting glass-to-glass and liquid-to-liquid phase transitions in supercooled water using non-classical nucleation theory,. *Chem. Phys.* 2018, Vol. 500, pp. 45-53.

46. **Tournier R.F.** Amorphous ices. [ed.] Pascal Richet. *Encyclopedia of Glass Science, Technology, History, and Culture,.* Hoboken : Wiley & Sons, 2021, Vol. 1, 3.14.

47. —. Homogeneous nucleation of phase transformations in supercooled water. *Physica B.* 2020, Vol. 579, p. 411895.

48. **Angell, C.A. and Rao, K.J.** Configurational excitations in condensed matter and the "bond lattice". Model for the liquid-glass transition. *J. Chem. Phys.* 1972, Vol. 57, pp. 470-481.

49. **Ozhovan, M.I.** Topological characteristics of bonds in SiO_2 and GeO_2 oxide systems at glass-liquid transition. *J. Exp. Theor. Phys.* 2006, Vol. 103 (5), pp. 819-829.

50. **Tournier R.F. and Ojovan M.I.** Undercooled phase behind the glass phase with superheated medium-eange order above glass transition temperature. *Physica B.* 2021, Vol. 602, p. 412542.

51. **Khvan, A.V. et al.** Thermodynamic properties of Tin: Part I: Experimental investigations, ab-initio modelling of alpha-, beta-phase and a thermodynamic description for pure metal in solid and liquid state from 0 K. *Calphad.* 2019, Vol. 65, pp. 50-72.

52. **Kozyrev, N.V. and Gordeev, V.V.** Thermodynamic characterization and equation of state for solid and liquid lead. *Metals.* 2022, Vol. 12, p. 16.

53. **Alchagirov, B.B. and Chochaeva, A.** Temperature dependence of the density of liquid tin. *High Temp.* 2000, Vol. 38, pp. 44-48.

54. **Kamiya, A., Terasaki, H. and Kondo, T.** Precise determination of the effect of temperature on the density of solid and liquid iron; nickel, and tin. *American mineralogist.* 2021, Vol. 106, pp. 1077-1082.

55. **Assael, M.J. et al.** Reference data for the density and viscosity of liquid cadmium, cobalt, gallium, indium, mercury, silicon, thallium, and zinc. *J. Phys. Chem.* 2012, Vol. 42, 3, p. 033101.

56. **Stankus, S.V., Savchenko, I.V. and and Yatsuk, O.S.** The caloric properties of liquid bismuth. 2018, High Temperature, Vol. 56 (1), pp. 33-37.

57. **Froberg, M.C. and Weber, R.** Dichtemessugen an eisen-kupfe legierungen. *Prch. Eisenhuttenw.* 1964, Vol. 35, 5, pp. 877-899.

58. **Gronvold, F.** Enthalpy of fusion and temperature of fusion of indium, and redetermination of the enthalpy ofbfusion of tin. *J. Chem. Therm.* 1993, Vol. 25, pp. 1133-1144.

59. **Chen, H.S. and Turnbull, D.** The specific heat of tin and gallium in their stable and undercooled pure liquid states. *Acta Metallurgica.* 1968, Vol. 16, pp. 369-373.

60. **Bryant, C.A. and Keesom, P.H.** Low temperature specific heat of indium and tin. *Phys. Rev.* 1961, Vol. 123, p. 491.

61. **Badawi, W.A., Brown-Acquaye, H.A. and Eid, A.E.** Heat capacity and thermodynamic properties of Bismuth in the range 333 to 923 K. *Bull. Chem.Soc. Jpn.* 1987, Vol. 60, pp. 3765-3769.

62. **Miller, R.R.** *Liquid metal Handbook.* s.l. : Nuclear Energy Agency, 1954. OECD 2015 NEA N°7268.

63. **Ojovan, M.I.** Viscosity and glass transition in amorphous oxides. *Adv. Cond. Matter Phys.* 2008, Vol. 2008, p. Article ID 817829.

64. **Ojovan M.I., Louzguine Luzgin D.V.** Revealing Structural Changes at Glass Transition via Radial Distribution Functions. *J. Phys. Chem.* 2020, Vol. 124, 3186-3194.

65. **Ojovan, M.L. and Louzguine-Luzgin, D.V.** On structural rearrangement during the vitrification of molten copper. *Materials.* 2022, Vol. 15, p. 1313.

66. **Zhu, F.G., et al.** Internal friction method: suitable also for structural changes of liquids. *Mater. Sci. Eng. A.* 2004, Vol. 370, pp. 427-430.

Author Contributions: only one author.

Institutional Review Board Statement: Not applicable.

Informed Consent Statement: Not applicable.